DYNAMIC 3D MEASUREMENT OF TYRE-TERRAIN INTERACTION

A. Glenn Guthrie[a], Theunis R. Botha[a], Emilio Jimenez[b], P. Schalk Els[a] and Corina Sandu[b]

[a] *Vehicle Dynamics Group (VDG), Department of Mechanical and Aeronautical Engineering, University of Pretoria, Pretoria, 0002, South Africa. glenn.guth@gmail.com, theunis.botha@up.ac.za, Schalk.Els@up.ac.za*
[b] *Advanced Vehicle Dynamics Laboratory (AVDL), Department of Mechanical Engineering, Virginia Polytechnic Institute and State University, Blacksburg, VA 24061, United States. jimeneex@vt.edu, csandu@vt.edu*

Abstract

When studying terramechanics for wheeled vehicles it is important to understand the tyre-terrain interaction. However the tyre road interface is hidden from view by the terrain and tyre itself. This makes determining the interaction externally very difficult. Some progress has been made by embedding sensors in the terrain or the tyre carcass however these techniques only capture a very small number of points. The problem of measuring dynamic tyre deformation at the tyre road interface from inside the tyre has been tackled in previous papers, however in this paper we seek to extend these measurements to identify the impact that rolling tyres have on the terrain. This is accomplished by measuring the undeformed soil profile in front of a tyre, the carcass deformation inside the tyre and the deformed soil profile behind the tyre. Test data was captured with the so-called Tyre–Terrain Camera System (T2CAM) on the Terramechanics rig at Virginia Tech using prepared sandy loam as the deformed soil material. T2CAM consists of three calibrated stereo camera rigs, a six-component load cell, wheel angle sensor and wheel speed sensor. Computer vision techniques are used with the images to generate full three dimensional profiles of the two soil areas and the inside surface of the tyre as captured by the cameras. The testing aims to compare undeformed soil profile with the deformed soil profile with the added information about the contact patch area and wheel forces to quantify both the plastic and elastic soil deformation.

Keywords: Terrain Mobility, Dynamic tyre deflection, Digital image correlation, terrain deformation

1. Introduction

The interaction between a tyre and the terrain on which it drives has long been one of the core interests of the terramechanics field. When dealing with hard terrains the tyre carcass deforms as a result of the forces exerted on it by the terrain while terrain deformation is minimal. When dealing with soft terrain (such as soil, mud or snow) both the tyre and the terrain will deform which makes simulating vehicle behaviour more challenging. The mechanical properties of a soft terrain determine the magnitude of its deformation and it is therefore theorised that by measuring the terrain profile before and after a tyre has deformed has occurred the mechanical properties may be recovered. This work sets out to develop a measurement system capable of measuring the soil deformation before and after a tyre has rolled over a patch of soil (referred to as the plastic deformation). Previously rut depth has been measured using mostly mechanical methods such as Arvidsson and Ristic (1996) who used a measurement board with adjustable needles spaced 60mm apart which were lowered into tyre track to measure the depth at discrete points across the profile. Kurjenluoma et al. (2009) used two adjacent Peiseler wheels (one running in the rut and one running on virgin ground) to measure the continuous depth of a rut. Botta et al., (2009) used long vertical rods (25mm apart) sliding through holes in an iron bar which was placed

across a tyre track to determine the rut depth. Line scan lasers may also be used to measure the rut depth however literature on the subject is mainly concerned with measurement of damage on hard roads and pavement for maintenance purposes.

Also of interest in this work is the elastic deformation of the soil since there will be a spring back effect after the tyre has passed over it (referred to as the elastic deformation). To calculate the elastic deformation of the soil the profile of the deformed tyre needs to be measured and the most common technique to directly measure the tyre deformation is to measure the profile on the inner surface of the tyre. Various methods of measuring the inner deformation have been used such as Magori, et al., (1998); Matsuzaki, et al., (2010); Xiong and Tuononen, (2015) who measured single points around the tyre surface or Green (2011) who used camera systems to measure a few discrete points. To recover elastic deformation however, the full inner profile is required.

This work uses the so called Tyre-terrain Camera System (T2CAM), which measures the deformation of the inside of the tyre carcass which is in contact with the terrain by Guthrie, et al., (2016) to determine the soil's elastic deformation. This is accomplished by adding three additional stereo camera pairs to measure the terrain before and after deformation. The measurements from the inner carcass measurement system is used to create a mapped profile of the outer tyre surface using the assumption that the tyre tread is compression is negligible when compared to carcass deformation. This allows plastic and elastic deformation of the soil to be determined.

2. Hardware Description

The measurement system consisted of four sets of stereo cameras positioned around the wheel. The first set of cameras was placed in front of the wheel and oriented directly downward to capture the undeformed terrain profile. A second set was oriented similarly and placed behind the wheel to capture the deformed terrain profile. A third set was positioned so that they would view the soil and tyre sidewall to facilitate slip measurement. Finally the last set of cameras was positioned inside tyre to view the contact patch.

The stereo cameras in T2CAM which view the contact patch are stabilised using a system of planetary gears (shown in Fig. 1) which ensures that the cameras inside the tyre view the contact patch at all times as the wheel rotates. The system consists of two large rings gears with 174 teeth each that are mounted on rollers which allow the rings to rotate about the rim's main axis of rotation. One of the large gears is mounted on the inside of the rim and the other is mounted on the outside of the rim. These gears each mesh with a pinion gear. The pinion gears are rigidly mounted to a shaft which passes through the wall of rim. The pinion shaft is mounted in a bearing housing with radial seals which stop air from escaping the inflated wheel. Having two gear sets with identical ratios connected together with a common shaft creates a gear system that constrains the two rings to rotate at the same angular velocity. Since the two large gears must always rotate at the same angular velocity it is possible to keep the inner ring stationary by simply holding the outer ring stationary.

Each stereo camera rig consists of two Pointgrey Flea3 (FL3-U3-13Y3M-C) high speed USB3 cameras (PointGrey, 2015) having a resolution of 1280x1024 with KOWA LM4NCL (Kowa, 2015) wide angle lenses. The cameras were connected via USB3 to a FitPC Mintbox Mini (FitPC, 2015) single chip computer which runs a modified version of the Linux Mint operating system which saved the images as video files.

The Mintbox which was located inside the wheel was mounted on the inner ring gear inside the tyre and accessed with a WiFi connection. The inner cameras were triggered to capture images via a proximity sensor which toggled between low and high voltage at discrete wheel rotations. The proximity trigger signal resulted in images being captured every 8.28° which corresponded to a longitudinal offset of 45 mm between samples. Lighting was provided by a 9W bank of LEDs powered by a 1 amp LED current driver. Power was introduced into the tyre via a set of copper slip rings which were integrated into the inner ring gear. Three pairs of graphite brushes (located at 120°intervals in the rim) slide along the slip rings to ensure that the power was never interrupted while the wheel the rotated.

The cameras outside the tyre were sampled simultaneously via a trigger signal from a central data acquisition unit. The tyre used in all tests on this system was a Michelin LTX A/T^2 LT235/85/R16.

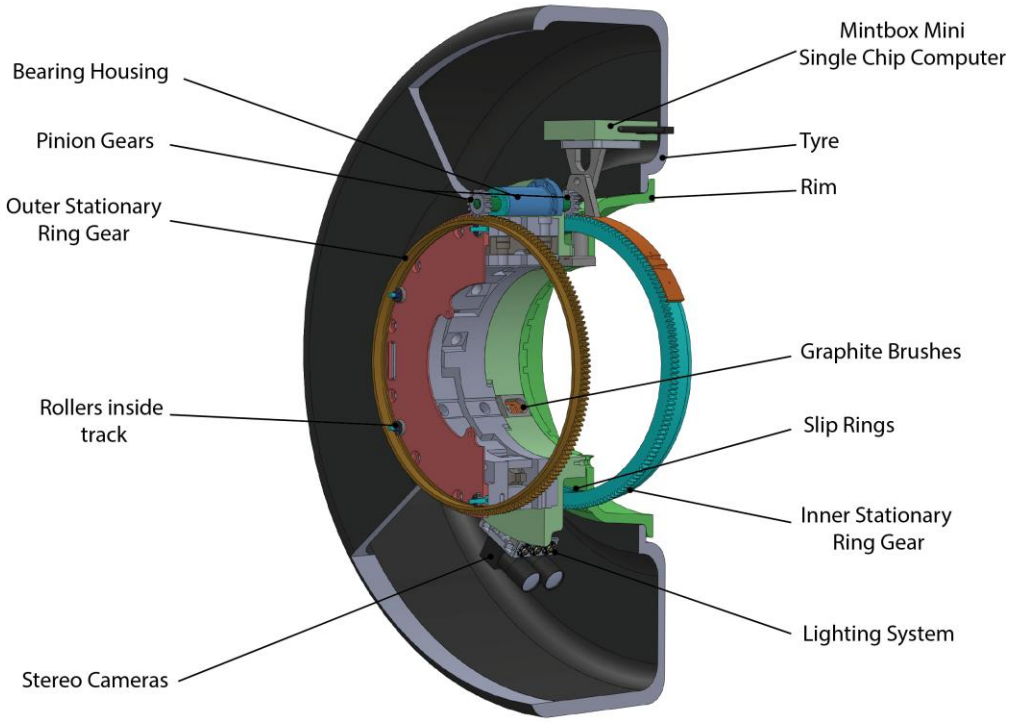

Fig. 1. The stabilisation system used inside the tyre to ensure that the cameras viewed the contact patch at all times.

3. Image Processing

A stereo pair of cameras can be used to determine the 3D position of a point visible to both cameras. If the same real world location is identified in both cameras, this point can then be triangulated from the 2D camera locations to its 3D real world location specified relative to the cameras. This method is graphically illustrated in Fig. 2. Therefore, the problem of determining the 3D locations of all points in a scene resolves around the problem of identifying the same region in both cameras. This process is called registration. The more accurate the registration process the more accurate the 3D location. An additional process which is performed is the calibration and distortion removal of the cameras. In order to perform the triangulation the relative location and rotation between the cameras need to be known as well as the focal length of the cameras. The lens distortion also needs to be removed to prevent the lens from affecting the results. This process is known as camera calibration and is easily performed using known calibration surfaces.

The surface profile of the terrain as well as the inside of the tyre is determined by using digital image correlation. The full field deformation measurement problem is solved by performing sub-pixel registration between the left and right images of a stereo pair. The left image is split into equally spaced square subsets. The subsets of the left image are mapped onto the right image by optimising a correlation metric between the subset in the left image and the right image. The concept is very similar to the Sum of Absolute Differences (SAD) metric often used in stereo correspondence matching. However, since deformation can occur between the left and right image due to camera orientation the subset is allowed not only to have vertical and horizontal displacement but is allowed to deform as well. The correlation metric is the zero-mean normalized sum of squared difference (ZNSSD) given as:

$$ZNSSD = \sum \left[\frac{f\left(x_{\Re f_{ij}}, y_{\Re f_{ij}}\right) - f_m}{\sum \left[f\left(x_{\Re f_{ij}}, y_{\Re f_{ij}}\right) - f_m \right]^2} - \frac{g\left(x_{cur_{ij}}, y_{cur_{ij}}\right) - g_m}{\sum \left[g\left(x_{cur_{ij}}, y_{cur_{ij}}\right) - g_m \right]^2} \right]^2 \qquad 3$$

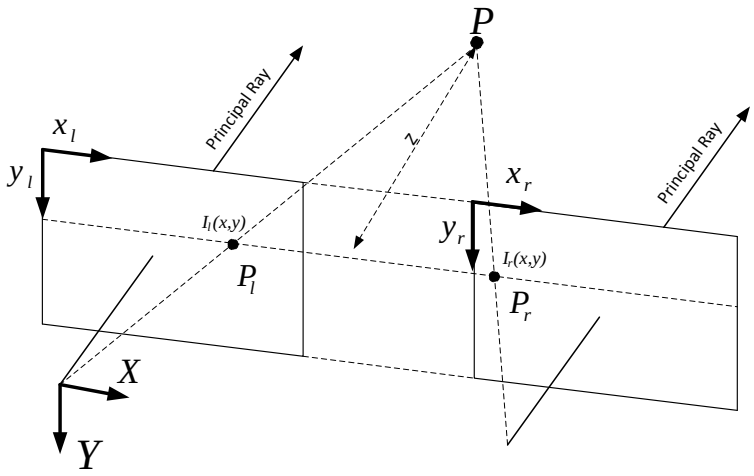

Fig. 2. Stereo vision methodology showing 3D point projected onto the left and right image planes

Where $f\left(x_{\Re f_{ij}}, y_{\Re f_{ij}}\right)$ is the grayscale value in the left image at location $x_{\Re f_{ij}}, y_{\Re f_{ij}}$, $g\left(x_{cur_{ij}}, y_{cur_{ij}}\right)$ is the grayscale image of the right image, f_m and g_m are the means of the subset in the left and right image respectively. The grayscale values are often needed at non integer locations, therefore the bicubic interpolation method is used to get sub pixel grayscale values. The coordinates in the reference image and current image are related as:

$$x_{cur\,ij} = x_{ref\,ij} + u + \frac{du}{dx}\left(x_{ref\,ij} - x_{ref\,c}\right) + \frac{du}{dy}\left(y_{ref\,ij} - y_{ref\,c}\right) \quad 4$$

$$y_{cur\,ij} = y_{ref\,ij} + v + \frac{dv}{dx}\left(x_{ref\,ij} - x_{ref\,c}\right) + \frac{dv}{dy}\left(y_{ref\,ij} - y_{ref\,c}\right) \quad 5$$

Where $x_{\Re f_{ij}}, y_{\Re f_{ij}}$ is the location of a point (i, j) in the subset and x_{cur}, y_{cur} are the location of the subset centre. The deformation vector $p = \left[u \quad v \quad \frac{du}{dx} \quad \frac{du}{dy} \quad \frac{dv}{dx} \quad \frac{dv}{dy}\right]^T$, which contains displacement components as well as the gradients of the displacement components, are the values being solved for each subset. The deformation vector is solved using the iterative non-linear Gauss-Newton algorithm. The algorithm used is called the inverse compositional Gauss-Newton method (IC-GN) method proposed by Baker and Mattews, (2004, 2001). The Gauss-Newton optimisation procedure requires an initial estimate which is close to the final value to assure convergence. The method developed at the University of Pretoria uses the Speeded Up Robust Features (SURF) Bay, et al., (2008) feature tracking algorithm to obtain an initial seed point for the first subset. Once the solution to the subset is found the neighbouring 4 subsets are solved using the displacement components of the already solved subset as an initial guess. The neighbouring subset with the best correlation value is then selected and its neighbouring subsets are solved for. This process continues until all subsets have been solved for.

This process provides the pixel locations of the subsets in both of the images and yields the location of each subset centre in both images. Using the stereo pair the 3D location of the subset can be found by using triangulation. The linear least squares method (Hartley and Sturm, 1997) is used to triangulate the stereo image correspondences to obtain the 3D location. This process, when applied to the front, rear and inside cameras, yields the 3D profile of the undeformed, deformed as well as the deformation of the inside of the tyre respectively . However, since it is required to have the outside profile of the tyre the inside profile is used with the thickness of the tyre to obtain the outside profile. The assumption is made that the compression of the carcass is negligible when compared to the global displacement of the tyre carcass and the soil. The thickness is obtained from a dissected tyre obtaining a profile of the tyre thickness as a function of the lateral displacement of the tyre. The thickness of the tyre is added to the inside profile by first determining the normal vector of the inside profile. The tyre thickness is then added in the direction of the normal vector. The normal vector at a point is obtained by using multiple surrounding points. The normal vector is determined as the eigenvector corresponding to the smallest eigenvalue of the points. The singular value decomposition of the points are taken to obtain the eigenvectors and eigenvalue as:

$$[UDV_t] = SVD(X - \bar{X})$$

where X is the 3 dimensional points and $\bar{X}$ is the mean of the points. The returned matrix D contains all the eigenvalues and U the eigenvectors. Once the normal vector is obtained the point is moved to the outside by multiplying the thickness with the normal vector. In this manner the outside profile of the tyre is obtained without including the tread pattern of the tyre.

4. Testing and Results

The testing was performed on Virginia Tech's Terramechanics test rig (Naranjo, et al., 2014). The rig ensures a constant vertical force even over uneven terrain. Longitudinal speed as well as wheel rotation can be accurately controlled to produce a desired slip ratio. The soil in the test rig was sandy loam which was tilled and compacted with a roller before every test run. Markings were made on the inside and outside of the tyre at 10° increments to facilitate alignment between internal and external cameras. The marked tyre can be seen doing a test run in Fig. 3

Each test consisted of capturing images from all cameras and measurements from the test rig itself while the rig moved at a constant longitudinal velocity and increasing wheel slip. Images were processed using the stereo algorithm from Section 3 to produce files containing millions of sample points (referred to as a point cloud). Each sample point is the 3D coordinates of a point on the measured surface with reference to the coordinate system of the left stereo camera. The cameras measuring the undeformed and deformed soil profiles were offset from one another therefore it was necessary to determine the relative distance and rotation between the two point clouds because each camera measures relative to its own coordinate system. Alignment was performed by importing the point clouds into CloudCompare (CloudCompare, 2016) which allowed the clouds to be easily manipulated. Each point in the cloud was coloured with its original pixel intensity from the left camera image so that common points were easily distinguishable. These points were used to manually translate and rotate the clouds to lie on top of one another which was a tedious process for large numbers of point clouds. This process may be improved in future by using the iterative closest point (ICP) methods developed by Botha, (2014)

Fig. 3. Complete system undergoing testing in the terramechanics rig at Virginia Tech. Visible in the top left are the cameras responsible for measuring the profile in front of the tyre

Fig. 4 shows an undeformed soil profile in front of the tyre that has been coloured to reflect the captured image. This area of soil captures a transition from tilled-uncompacted soil to a tilled-compacted region. This area was chosen because it contained many unique features which were useful in the alignment process. This alignment process could have been made easier by measuring the distance between the cameras during testing so that the translation and rotation were always constant. The point cloud of the undeformed soil shows the flat compacted region and the rough uncompacted zone. Fig. 5 shows the plastically deformed soil profile at the same location with most of the rough uncompacted features formed into a rut. The two profiles were compared by generating a smooth mesh from the undeformed point cloud which could be used to calculate a signed perpendicular distance (C2M) between the two clouds. The deformed points are assigned a colour based on their distance (in mm) from the undeformed mesh surface. The sign of this displacement is said to be

positive if the deformed profile point perpendicular to the reference surface is located perpendicular to the bottom of the reference surface and negative if the point is perpendicular to the top of the reference surface.

Fig. 6 shows the deformed profile with the signed distances. The colour map shows that the area of highest plastic deformation was the region under the transition from the compacted to uncompacted soil where a bank had been pushed up by the roller. The area with the second highest deformation was in the tread pattern which matches expectations. There are outliers however with a large amount of negative deformation being shown in some areas. This is partly due to the deformed profile being captured in lower light conditions and partly to the alignment issues discussed earlier.

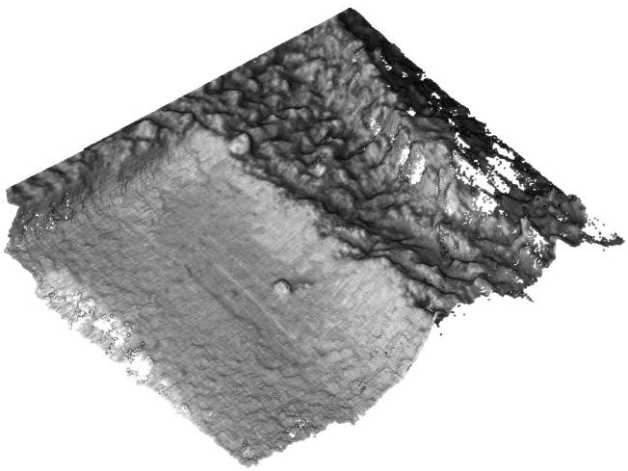

Fig. 4. The point cloud of the undeformed soil in front of the tyre coloured to match the input images.

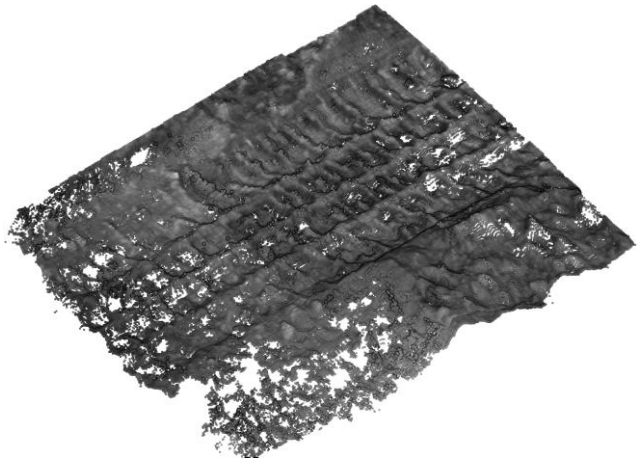

Fig. 5. The point cloud of the deformed soil behind the tyre coloured to match the input images.

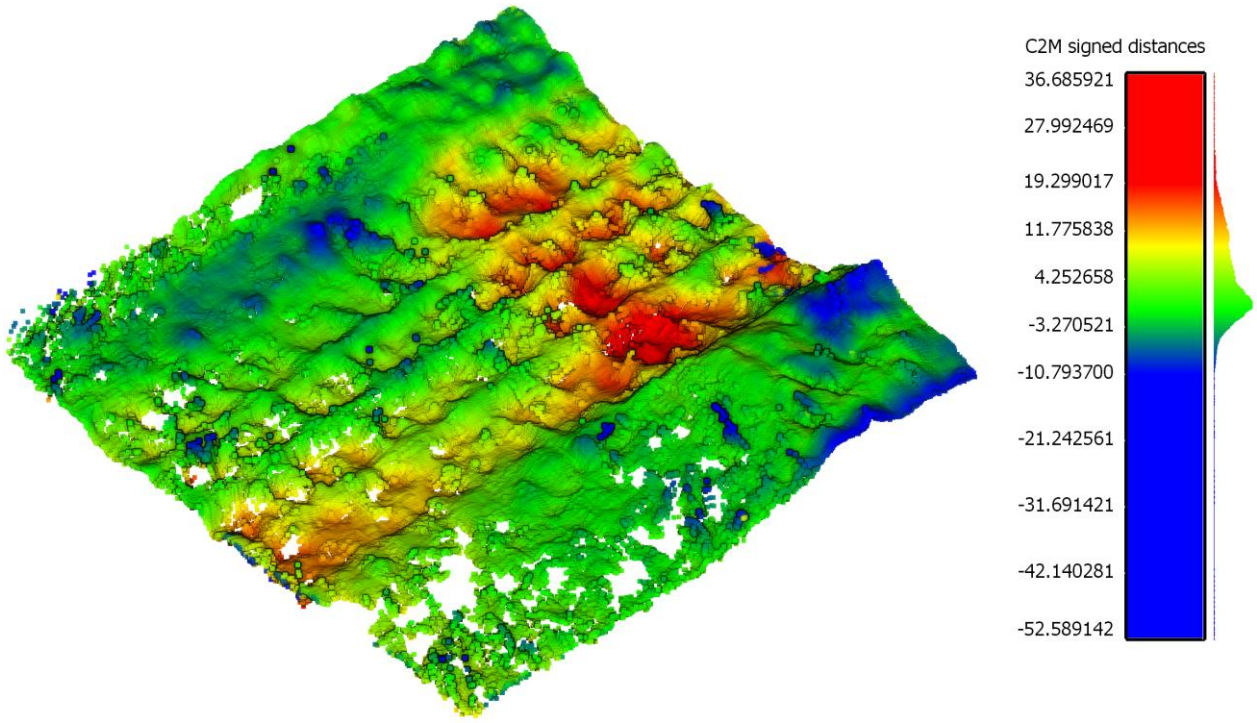

Fig. 6. The deformed point cloud with a colour map applied to represent the relative distance to the undeformed profile

The second part of the study involved attempting to recover the outer profile of the tyre using the measured inner profile. Fig. 7 shows a smooth ideal outer profile of the tyre which was obtained using the method explained in Section 3. The outer profile of the tyre does not include the tread because the tread blocks are irregularly spaced and it proved challenging to accurately map their position on the outer surface to an inner location.

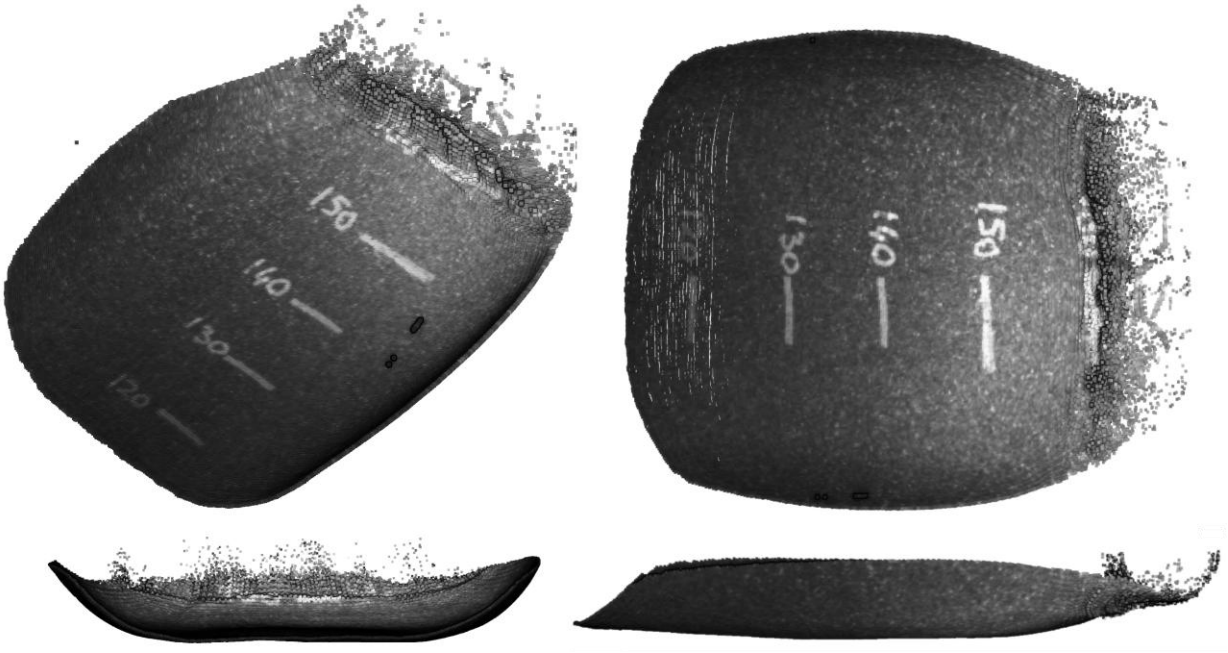

Fig. 7. Four views of the outer tyre profile generated from measurement of the inner tyre surface

To test the viability of this technique as a means to determine elastic soil deformation the difference between the measured elastic and plastic deformation was computed by measuring the distance between the outer tyre profile and the plastically deformed soil profile. To perform this calculation the tyre profile was aligned with the deformed soil profile using video of the sidewall of the tyre passing through the compaction boundary and finding the inner profile whose markings matched the markings on the sidewall. When the tyre profile was placed at this location (shown in Fig. 8) it was observed that some points in the deformed soil profile were above the blue tyre profile due partly to the tread blocks being absent and partly to the elastic component of the soil deformation.

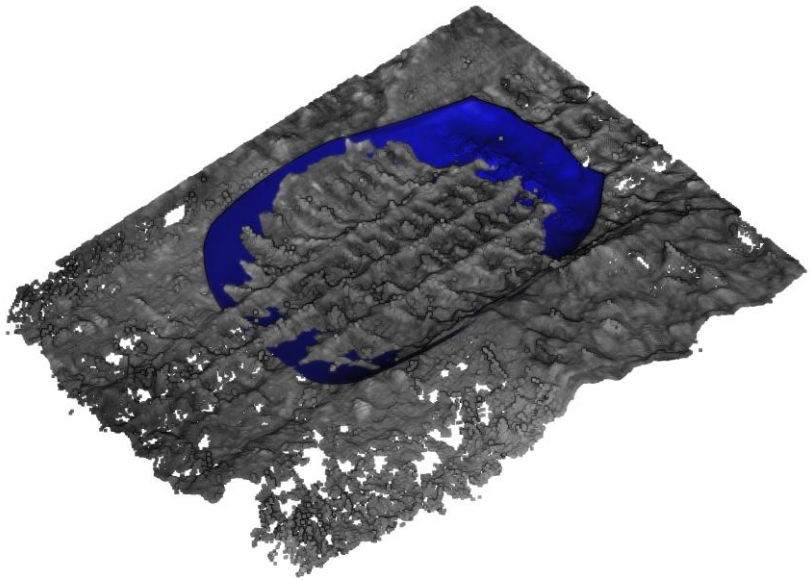

Fig. 8. The deformed soil point cloud and the outer tyre profile after alignment using the side cameras.

Fig. 9 shows a colour plot of the relative distance between a mesh made from the tyre profile and the deformed soil. The colour plot represents any point which is theoretically inside the tyre surface or being elastically deformed. It should be noted that because the tread is neglected the high points on the tread pattern will have artificially high values.

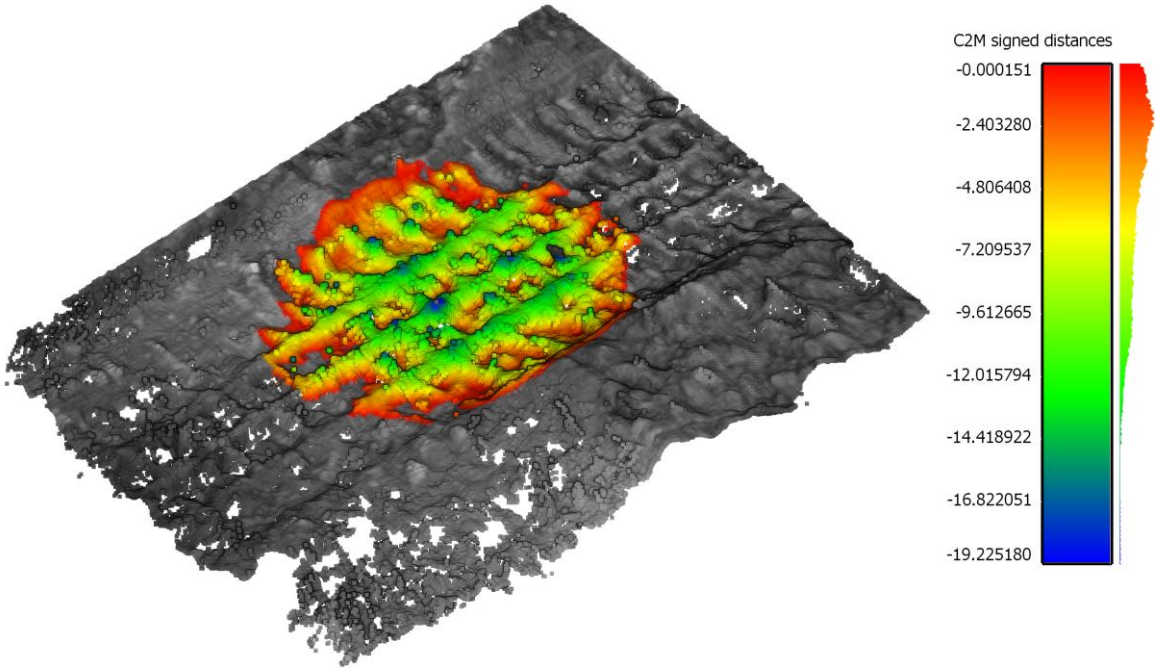

Fig. 9. Point cloud of the deformed profile showing the distance between the tyre profile that caused the deformation and the final measured deformation.

5. Conclusion

The aim of this study was to determine the viability of stereo camera measurement techniques as a means of quantifying soft terrain deformations. The T2CAM system combined with 3 eternal stereo camera rigs was able to accurately measure the undeformed and deformed soil profile from images as well as recover the outer tyre profile from inner camera measurements. These soil profile measurements were used to generate a distance measure to quantify how much the soil had been deformed by the tyre. The tyre profile was used with the deformed profile to create a measure of how much elastic deformation is experienced by the soil as the tyre rolls over it. This measure proved problematic due to the difficulty of adding tread blocks to the tyre profile creating artificial peaks where the tread impression had been measured. Overall the technique shows significant promise as a means of measuring soil deformations and providing accurate full field rut measurements which could not be performed previously.

Future work requires adding more sensors to the system to allow the measurements to be validated, doing more precise relative measurements so that alignment can be more accurate and finding a way to synchronise the measurements from inside and outside the tyre. Once the system has undergone further testing it may be possible use the deformation information to create discrete element models and quantify soil parameters.

Nomenclature

$\frac{du}{dy}$	Horizontal displacement gradient in y-axis	$\frac{dv}{dy}$	Vertical displacement gradient in y-axis	
$\frac{dv}{dx}$	Vertical displacement gradient in x-axis	$\frac{du}{dx}$	Horizontal displacement gradient in x-axis	
$f(x,y)$	Grayscale of reference image at pixel coordinates (x, y)	$x_{ref_{ij}}$	Reference image x-coordinate of subset particle i, j	[pixel]
$g(x,y)$	Grayscale of current image at pixel coordinates (x, y)	$y_{ref_{ij}}$	Reference image y-coordinate of subset particle i, j	[pixel]

f_m	Average grayscale value of subset in reference image		$x_{cur_{ij}}$	Current image x-coordinate of subset particle i, j	[pixel]
g_m	Average grayscale value of subset in current image		$y_{cur_{ij}}$	Current image y-coordinate of subset particle i, j	[pixel]
u	Horizontal displacement component	[pixels]	x_{ref_c}	Subset x-centre of reference image	[pixel]
v	Vertical displacement component	[pixels]	y_{ref_c}	Subset y-centre of reference image	[pixel]

Acknowledgements

The research leading to these results has received funding from the European Union Horizon 2020 Framework Program, Marie Sklodowska-Curie actions, under grant agreement no. 645736.

References

Arvidsson, J., and Ristic, S., 1996. Soil stress and compaction effects for four tractor tyres. J. Terramechanics 33, 223–232. doi:10.1016/S0022-4898(97)00006-2

Baker, S., and Mattews, I., 2004. Lucas-Kanade 20 years on: a unifying framework. Int. J. Comput. Vis. 56, 221–255.

Baker, S., and Mattews, I., 2001. Equivalence and efficiency of image alignment algorithms, in: IEEE Conference Computer Vision Pattern Recognition. pp. 1090–1097.

Bay, H., Ess, A., Tuytelaars, T., and Van Gool, L., 2008. Speeded-Up Robust Features (SURF). Comput. Vis. Image Underst. 110, 346–359. doi:10.1016/j.cviu.2007.09.014

Botha, T.R., 2014. Digital Image Correlation : Applications in Vehicle Dynamics. University of Pretoria.

Botta, G.F., Becerra, A.T., and Tourn, F.B., 2009. Effect of the number of tractor passes on soil rut depth and compaction in two tillage regimes. Soil Tillage Res. 103, 381–386. doi:10.1016/j.still.2008.12.002

CloudCompare, 2016. Cloud Compare [WWW Document]. URL http://www.cloudcompare.org/ (accessed 3.24.16).

FitPC, 2015. MintBox Mini [WWW Document]. URL http://www.fit-pc.com/web/products/mintbox/mintbox-mini/ (accessed 2.16.16).

Green, R.W., 2011. A Non-contact Method for Sensing Tire Contact Patch Deformation Using a Monocular Vision System and Speckled Image Tracking. Auburn University.

Guthrie, A.G., Botha, T.R., Becker, C.M., Els, P.S., Sopher, A., and Shoop, S., 2016. Measurement of tire carcass inside deformation, in: 8th Americas Regional Conference of International Society for Terrain- Vehicle Systems. p. 40.

Hartley, R.I., and Sturm, P., 1997. Triangulation. Comput. Vis. Image Underst. 68, 146–157.

Kowa, 2015. Kowa LM4NCL [WWW Document]. URL http://www.kowa.eu/lenses/en/products.php (accessed 5.24.15).

Kurjenluoma, J., Alakukku, L., and Ahokas, J., 2009. Rolling resistance and rut formation by implement tyres on tilled clay soil. J. Terramechanics 46, 267–275. doi:10.1016/j.jterra.2009.07.002

Magori, V., Magori, V.R., and Seitz, N., 1998. On-line determination of tyre deformation, a novel sensor principle, in: Ultrasonics Symposium, 1998. Proceedings., 1998 IEEE. pp. 485–488.

Matsuzaki, R., Hiraoka, N., Todoroki, A., and Mizutani, Y., 2010. Optical 3D Deformation Measurement Utilizing Non-planar Surface for the Development of an "Intelligent Tire." J. Solid Mech. Mater. Eng. 4, 520–532.

Naranjo, S., Sandu, C., and Taheri, S., 2014. Experimental testing of an off-road instrumented tire on soft soil. J. Terramechanics 56, 119–137.

PointGrey, 2015. Point Grey Flea3 1.3 MP Mono USB3 Camera [WWW Document]. URL http://www.ptgrey.com/flea3-13-mp-mono-usb3-vision-vita-1300-camera (accessed 5.24.15).

Xiong, Y., and Tuononen, A., 2015. Rolling Deformation of Truck Tires : Measurement and Analysis Using a Tire Sensing Approach. J. Terramechanics 61, 33–42. doi:10.1016/j.jterra.2015.07.004